UARI Research Report No. 28

HYPERSONIC FLOW OF AIR PAST A CIRCULAR CYLINDER WITH NON-EQUILIBRIUM OXYGEN DISSOCIATION INCLUDING DISSOCIATION OF THE FREE STREAM

by

Rudolf Hermann and Jurgen Thoenes

Paper presented at the
VI. EUROPEAN AERONAUTICAL CONGRESS
at Munich, Germany, September 1-4, 1965

This work was partially supported by the
National Aeronautics and Space Administration
under research grant NsG-381

UNIVERSITY OF ALABAMA RESEARCH INSTITUTE
Huntsville, Alabama

September, 1965

UARI Research Report No. 28

HYPERSONIC FLOW OF AIR PAST A CIRCULAR CYLINDER WITH NON-EQUILIBRIUM OXYGEN DISSOCIATION INCLUDING DISSOCIATION OF THE FREE STREAM

by

Rudolf Hermann and Jurgen Thoenes

Paper presented at the
VI. EUROPEAN AERONAUTICAL CONGRESS
at Munich, Germany, September 1-4, 1965

This work was partially supported by the
National Aeronautics and Space Administration
under research grant NsG-381

UNIVERSITY OF ALABAMA RESEARCH INSTITUTE
Huntsville, Alabama

September, 1965

ABSTRACT

12861

Hypersonic, chemically relaxing inviscid flow of air past a circular cylinder has been calculated using Dorodnitsyn's method of integral relations. Considered are the effects of non-equilibrium oxygen dissociation on the distribution of the flow variables in the subsonic and supersonic region of the shock layer. Also investigated is the influence of oxygen dissociation in the free stream on the shock detachment distance and the flow field in general.

Particular emphasis has been placed on the investigation of the flow along the stagnation streamline, which indicates the existence of an equilibrium region in front of the body. Its size depends strongly on the density, on the body size, and on the magnitude of the reaction rate constants. The numerical integration of the equations for the flow around the body does not readily yield the shock detachment distance on the stagnation streamline. An iteration procedure has to be used until a stagnation shock detachment distance is found such that the derivatives of all variables are continuous across the sonic line.

The results show that the shock wave, at fixed free stream composition, moves closer to the body with increasing free stream Mach number, that is with larger oxygen dissociation behind the shock. However, increasing oxygen dissociation in the free stream, at otherwise fixed free stream conditions, pushes the shock wave away from the body.

author

TABLE OF CONTENTS

LIST OF FIGURES

NOMENCLATURE

b	Oxygen mole fraction in undissociated air, defined in eq. (2.1)
C	Number of oxygen atoms per unit mass of gas
D	Dissociation energy [J/kmol]
D'	Characteristic temperature of dissociation [^oK]
E	Total internal energy [J/kg]
e	Specific internal energy [J/kg]
f_i	Mole fraction of ith species
F	Source function
h	Enthalpy [J/kg]
K_c	Concentration equilibrium constant [particles/m^3]
k_d	Dissociation rate constant [m^3/particle · sec]
k_r	Recombination rate constant [m^6/particle^2 · sec]
M	Molecular weight of undissociated gas
M_i	Colliding Body (ith species)
N_A	Avogadro's number [kmol^{-1}]
$\vec{n}$	Unit normal vector
n_i	Number density of ith species (undissociated gas)
$\bar{n}_i$	Number density of ith species (dissociated gas)
O	Oxygen
p	Pressure [N/m^2]
$\vec{q}$	Velocity vector
R	Gas constant of undissociated gas [J/kg ^oK]
R^*	Universal gas constant [J/kmol ^oK]
r	Radial coordinate

S	Surface $[m^2]$
T	Temperature $[^oK]$
t	Time [sec]
u,v	Velocity components in circumferential and radial direction, respectively [m/sec]
V	Volume $[m^3]$
w	Net rate of production of oxygen atoms per unit volume of gas
Z	Compressibility factor
α	Degree of oxygen dissociation
Δ	Shock detachment distance
$\epsilon = \Delta/r_b$	Shock detachment distance (dimensionless)
$\eta = r/r_b$	Radial coordinate (dimensionless)
θ	Circumferential coordinate
θ_i	Vibrational temperature of ith species $[^oK]$
ρ	Mass density $[kg/m^3]$
σ	Shock wave angle

Subscripts

1	Free stream
b	Body surface
M	Colliding body
N2	Nitrogen
n	Normal component
O	Atomic oxygen
O2	Molecular oxygen
o	Stagnation point
t	Tangential component, also total conditions
s	Behind shock wave

INTRODUCTION

The importance of blunted shapes in the hypersonic flight of a vehicle re-entering the atmosphere from outer space has led to many investigations of hypersonic flows with detached shock waves, using both inverse and direct methods. In the inverse method the flow field around the body is determined by specifying a certain shock shape, and the associated body shape follows from the calculation. This method has the advantage that the problems associated with the specification of boundary conditions along an unknown shock wave are avoided. Although it has been successfully applied, for example by Hall (Ref. 1), even for real gas, the method is extremely tedious if the flow field around a given body shape has to be determined.

In 1959 Dorodnitsyn (Ref. 2) has described a method of integral relations for the solution of two-dimensional boundary value problems. This method is also applicable to problems with free boundaries and has first been applied by Belotserkovskii (Ref. 3) to the calculation of supersonic flow of a perfect gas past a circular cylinder. Also using a perfect gas, this basic work has been extended by various other authors (Ref. 4, 5, 6) for other body shapes.

The assumption of a perfect gas is customary for flight speeds where the kinetic energy of the flow does not appreciably excite internal degrees of freedom of the particles composing the gas. At hypersonic velocities as they are encountered during re-entry, a considerable fraction of the free stream kinetic energy is transformed into thermal

energy behind the bow shock, causing excited molecular vibration, dissociation, and even ionization. In modern high speed flow facilities designed to simulate such flight conditions, this highly excited state is already reached in the nozzle supply chamber, causing frozen dissociation in the nozzle test section (Ref. 7, 9). It is the coupling of these so-called real gas effects, as described above, with the usual flow processes that is responsible for the difficulties encountered in the flow field calculations of vehicles flying at hypersonic speeds.

Up to the present time, only a limited number of investigators have obtained results for real gas flows in connection with the integral method. The first results where presented by Shih, Baron, e.a. (Ref. 8), for hypersonic non-equilibrium flow of air past a sphere. Simultaneously, Yalamanchili and Hermann (Ref. 7, 9) investigated non-equilibrium flow of air past a circular cylinder. It must be mentioned here that results from this investigation, also published in Ref. 9, were found to be incorrect due to an error in the computer program. However, the equations are correct as published. Later Belotserkovskii, e.a. (Ref. 10), used the integral method to calculate equilibrium flow of air past spheres and ellipsoids.

In the present paper, new results are given for non-equilibrium hypersonic flow of air past a circular cylinder. Also treated is, for the first time to the authors' knowledge, the case of dissociation in the free stream. Such conditions are encountered, either in the atmosphere at high altitudes, or in the nozzle of heated flow facilities where appreciable frozen dissociation may occur.

GAS MODEL AND THERMODYNAMIC EQUATIONS

2.1 Gas Model

The simplified air model used in this investigation consists of oxygen atoms, oxygen molecules and nitrogen molecules only. In other words, the range of application is such that only oxygen may dissociate. The formation of nitric oxide is neglected. While the oxygen content was very closely approximated, the remaining gases in atmospheric air, mainly argon and carbon dioxide, were added to the nitrogen fraction of our gas model. Specifically, the mole fraction of oxygen in undissociated air was chosen as

$$b = \frac{n_{02}}{n_{02} + n_{N2}} = 0.21 \tag{2.1}$$

where n_i denote the number of particles of the ith species per unit volume of the gas.

This air model has been introduced by Hermann (Ref. 11), and it has been shown to be a reasonable approximation to real air in the appropriate range of temperatures and pressures (Ref. 12, 13). It permits us to gain an insight in the distinct features of non-equilibrium flow phenomena with a minimum of computational effort.

2.2 Thermal Equation of State

The degree of oxygen dissociation, α, is defined as the ratio of the mass of oxygen in dissociated form to the total mass of oxygen in the mixture. Assuming that the individual species of the mixture obey the perfect gas law, the pressure of the mixture is the sum of

its partial pressures, or

$$p = \sum_i p_i = \sum_i \rho_i R_i T \tag{2.2}$$

With the above definition and assumption, the thermal equation of state for the mixture can be derived as

$$p = \rho R Z T \tag{2.3}$$

where

$$Z = 1 + b\alpha \tag{2.4}$$

2.3 Internal Energy and Enthalpy

The internal energy of the gas mixture is the weighted sum of the internal energies of each species due to the various modes of excitation (translation, rotation, vibration) and the dissociation energy of the dissociating component,

$$E = \sum_i f_i e_i + \frac{f_O}{2} D_{O2} \tag{2.5}$$

where the f_i denote the mole fractions, and D_{O2} is the dissociation energy.

The enthalpy of the mixture is defined as

$$h = E + \frac{p}{\rho} \tag{2.6}$$

After determining the mole fractions, an explicit expression for the internal energy of the mixture can be obtained from statistical thermodynamics. Then, substituting (2.5) and (2.3) into (2.6), the enthalpy may be written as

$$h = R\left[b\alpha D'_{O2} + \frac{3}{2}\, b\alpha T + \frac{7}{2}\, T + (1 - \alpha)\,\frac{b\theta_{O2}}{e^{\theta_{O2}/T} - 1} + (1 - b)\,\frac{\theta_{N2}}{e^{\theta_{N2}/T} - 1}\right] \tag{2.7}$$

where R is the gas constant of undissociated air, θ_i the characteristic temperature of vibration, and D'_{O2} a characteristic temperature of dissociation. From the form of eq. (2.7), it should be noted that the molecular vibrations are assumed to be in equilibrium with the translations and rotations.

2.4 Rate Equation

In general, a large number of collisions among the particles are required to equilibrate dissociation (and other modes of excitation) with the local translational temperature. This means that a finite amount of time is needed for the gas to achieve thermodynamic equilibrium. The departure from equilibrium of a flowing gas is characterized by the magnitude of this relaxation time relative to some translational time needed by the particles to move over a certain distance. It is the purpose of this subsection to present the necessary equations that will enable us to account for such non-equilibrium effects in our calculations.

Since only oxygen dissociation is considered in this analysis, only one chemical rate equation is needed. For steady flow, let w be the net number of oxygen atoms generated per unit volume and unit time and $\bar{n}_O$ the number of free oxygen atoms per unit volume of the

fluid. For an arbitrary volume V, the net number of oxygen atoms generated per second must then be equal to the flux of free oxygen atoms across its boundary S, that is

$$\int_V w dV = \int_S \bar{n}_O \vec{q} \cdot \vec{n} dS \tag{2.8}$$

where $\vec{q}$ is the velocity and $\vec{n}$ a unit normal. Applying the divergence theorem to the right hand side, eq. (2.8) may be written as

$$\int_V [w - \nabla \cdot (\bar{n}_O \vec{q})] dV = 0 \tag{2.9}$$

Since the considered volume was arbitrary, we must have

$$\nabla \cdot (\bar{n}_O \vec{q}) = w \tag{2.10}$$

Defining now C as the number of oxygen atoms (in either molecular or atomic form) per unit mass of the gas,

$$C = \frac{2bN_A}{M} \tag{2.11}$$

we can express the number of free oxygen atoms per unit volume of the gas as

$$\bar{n}_O = C\alpha\rho \tag{2.12}$$

Substituting the above into eq. (2.10) and using the over-all continuity equation, which states that

$$\nabla \cdot (\rho \vec{q}) = 0 \tag{2.13}$$

the rate equation becomes simply

$$\vec{q} \cdot \nabla\alpha = \frac{w}{C\rho} \tag{2.14}$$

The net rate of oxygen atoms generated per unit volume of the fluid is

$$w = \left(\frac{d\bar{n}_O}{dt} \right)_{diss} + \left(\frac{d\bar{n}_O}{dt} \right)_{rec} \tag{2.15}$$

The equations for the reactions that may occur in the considered air model are of the form

$$O_2 + M_i \underset{k_{r,i}}{\overset{k_{d,i}}{\rightleftarrows}} 2O + M_i \tag{2.16}$$

where M_i symbolizes a particle of the ith species acting as colliding body necessary to either dissociate the molecule or recombine some atoms, and where $k_{d,i}$ and $k_{r,i}$ are the rate constants for the specific reaction. It is obvious then that eq. (2.16) represents a set of three different reactions, since M_i may be an oxygen atom or molecule, or a nitrogen molecule.

In order to simplify the calculations we shall now consider M_i to represent any particle of our gas mixture, the composition of which is given by the sum of the concentrations of the actual species. Denoting by $\bar{n}_M$ the number of particles per unit volume that may act as a colliding body, we have for our air model

$$\bar{n}_M = \bar{n}_O + \bar{n}_{O2} + \bar{n}_{N2} \tag{2.17}$$

From the law of mass action, it is known that the rate of change of concentration is proportional to the product of the concentrations, raised to the power of the stoichiometric coefficients. In the process of dissociation an oxygen molecule must collide with some other particle having enough energy to break up the oxygen molecule. For

the recombination of two atoms, a triple collision is necessary, the third body carrying away the energy that the two separate atoms must release to form a stable diatomic molecule. Hence, according to (2.15),

$$w = k_d \bar{n}_{O2} \bar{n}_M - k_r \bar{n}_O^2 \bar{n}_M \tag{2.18}$$

where k_d and k_r are the temperature dependent reaction rate "constants" for dissociation and recombination respectively. For local thermodynamic equilibrium, the net rate of oxygen atoms generated vanishes; i.e., $w = 0$; hence,

$$\frac{k_d}{k_r} = \frac{\bar{n}_O^2}{\bar{n}_{O2}} = K_c \tag{2.19}$$

where K_c is the concentration equilibrium constant for the considered reaction. Assuming now that the above relation is also valid when the flow is out of chemical equilibrium, the rate equation can finally be written as

$$\vec{q} \cdot \nabla\alpha = F \tag{2.20}$$

where

$$F = \frac{C^2 \rho^2 Z k_d}{2b} \left[\frac{1 - \alpha}{2C\rho} - \frac{\alpha^2}{K_c} \right] \tag{2.21}$$

In eq. (2.21) K_c is a function of temperature only; it is also obtained from statistical thermodynamics.

In order to evaluate the rate equation we still need expressions for the dissociation rate constant.

A comprehensive review of recent work carried out in the field of reaction rates was given by Wray (Ref. 14). His values for the various colliding bodies will be used in the present investigation.

As a consequence of the simplification that was introduced previously, it was necessary in eq. (2.18) to assume a single rate constant each for dissociation and recombination. In order to account for the influence of the catalyzing species, at least in a simplified fashion, it is therefore proposed to use as a dissociation rate constant, a population averaged expression of the form

$$k_d = \sum_i f_i k_{d,i} \tag{2.22}$$

where the f_i are the mole fractions and where the $k_{d,i}$ denote the dissociation rate constants (for oxygen) with the ith species acting as catalyst (see eq. 2.16). The resulting dissociation rate constant can then be expressed as

$$k_d = \frac{2.5 \cdot 10^8}{TN_A Z} \left(\frac{D_{02}}{R^*} \right)^{1.5} e^{-\frac{D_{02}}{R^*T}} (2 + 7b + 41\alpha b) \tag{2.23}$$

In this form the dissociation rate "constant" is seen to be a function of temperature and composition.

FLOW PAST A CIRCULAR CYLINDER

3.1 Basic Equations

Neglecting viscosity, heat conduction and radiation, the basic equations for steady, adiabatic flow are the following:

Conservation of mass:

$$\nabla \cdot (\rho \vec{q}) = 0 \tag{3.1}$$

Conservation of momentum:

$$\nabla \left(\frac{q^2}{2} \right) + (\nabla \times \vec{q}) \times \vec{q} + \frac{1}{\rho} \nabla p = 0 \tag{3.2}$$

Conservation of energy:

$$\vec{q} \cdot \nabla \left(h + \frac{q^2}{2} \right) = 0$$

or

$$h + \frac{q^2}{2} = h_t = \text{const.} \tag{3.3}$$

The above equations are the usual equations of motion, and they do not depend on any particular gas model. In order to solve these equations for the unknowns, they must be supplemented by a thermal equation of state and an expression for the enthalpy, which do depend on the particular gas model and were derived in the previous section as given in eq. (2.3) and (2.7).

If the gas under consideration is reacting, additional equations for the conservation of species (rate equations) must be added to the system. For our simplified air model, we have only one rate equation, namely,

$$\vec{q} \cdot \nabla \alpha = F \tag{3.4}$$

where F is the source function, given by eq. (2.21).

For the calculations that we have in mind, a polar coordinate system, referred to the center line of the cylinder, is the most suitable one (See Fig. 1.). The transformation of the equations from the vectorial form to polar coordinates is standard, and the result is as follows:

Conservation of mass:

$$\frac{\partial}{\partial\theta}(\rho u) + \frac{\partial}{\partial r}(\rho v r) = 0 \tag{3.5}$$

θ-momentum:

$$u\frac{\partial u}{\partial\theta} + vr\frac{\partial u}{\partial r} + uv + \frac{1}{\rho}\frac{\partial p}{\partial\theta} = 0 \tag{3.6}$$

r-momentum:

$$\frac{\partial}{\partial\theta}(\rho uv) + \frac{\partial}{\partial r}\left[(p + \rho v^2)r\right] - (p + \rho u^2) = 0 \tag{3.7}$$

Rate equation:

$$u\frac{\partial\alpha}{\partial\theta} + vr\frac{\partial\alpha}{\partial r} - Fr = 0 \tag{3.8}$$

The conservation of mass and the r-momentum equation are given in divergence form, which is required for the application of the integral method.

3.2 Boundary Conditions

The condition for flow tangency on the body surface is given by

$$v_b = 0 \tag{3.9}$$

The conditions behind the shock are obtained from the conservation of mass, momentum and energy across the shock:

Conservation of mass:

$$\rho_1 u_{n1} = \rho_s u_{ns} \tag{3.10}$$

Conservation of momentum:

$$u_{t1} = u_{ts} \tag{3.11}$$

$$\rho_1 u_{n1}^2 + p_1 = \rho_s u_{ns}^2 + p_s \tag{3.12}$$

Conservation of energy:

$$h_1 + \frac{u_{n1}^2}{2} = h_s + \frac{u_{ns}^2}{2} \tag{3.13}$$

where p and h are given by the equation of state, eq. (2.3), and the enthalpy equation, eq. (2.7), respectively.

3.2.1 Frozen Shock Conditions

For the present non-equilibrium flow calculations, it will be assumed that the composition of the air does not change across the shock; i.e., $Z_1 = Z_s$. Using this assumption and equations (2.3), (3.10), (3.12) and (3.13), one obtains easily

$$T_s = \frac{u_{n1}}{RZ_1}\left(1 + \frac{RZ_1T_1}{u_{n1}^2}\right)\sqrt{u_{n1}^2 - 2(h_s - h_1)} - \frac{2}{RZ_1}\left[\frac{u_{n1}^2}{2} - (h_s - h_1)\right] \tag{3.14}$$

For any given free stream conditions (i.e, T_1, α_1, u_{n1}), the temperature behind the shock, T_s, can now be obtained from eq. (3.14) and eq. (2.7) by solving these equations numerically. Using the continuity equation, eq. (3.10), and the energy equation, eq. (3.13), the density ratio across the shock is obtained as

$$\frac{\rho_s}{\rho_1} = \frac{u_{n1}}{\sqrt{u_{n1}^2 - 2(h_s - h_1)}} \tag{3.15}$$

Knowing the temperature and the density behind the shock, the static pressure ratio across the shock becomes

$$\frac{p_s}{p_1} = \frac{\rho_s}{\rho_1} \cdot \frac{T_s}{T_1} \tag{3.16}$$

which completes the calculations of the static conditions behind the shock. It may be mentioned that in Ref. 15 numerical results of the above calculations are given for a wide range of free stream conditions.

3.2.2 Geometric Relations

For the calculations ahead, the velocity behind the shock must be given in the present coordinate system. From Fig. 1, one obtains

$$u_s = - u_{ns} \cos(\sigma + \theta) + u_{ts} \sin(\sigma + \theta) \tag{3.17}$$

$$v_s = - u_{ns} \sin(\sigma + \theta) - u_{ts} \cos(\sigma + \theta) \tag{3.18}$$

where the velocity components as referred to the locally oblique shock are given by

$$u_{ts} = u_{t1} = u_1 \cos \sigma \tag{3.19}$$

$$u_{ns} = u_1 \left(\frac{\rho_1}{\rho_s} \right) \sin \sigma \tag{3.20}$$

Fig. 1 also indicates that the relation between the shock wave coordinates and the shock wave angle σ is given by

$$\frac{d\Delta}{d\theta} = - (r_b + \Delta) \cot(\sigma + \theta) \tag{3.21}$$

where σ and Δ are functions of θ.

3.3 Application of the One-Strip Integral Method

The method of integral relations, proposed by A. A. Dorodnitsyn (Ref. 2), and first applied by Belotserkovskii (Ref. 3), is already well known. Its application to the calculations of hypersonic flow past blunt bodies was also explained in Ref. 9 and will not be repeated here. In contrast to the description given in Ref. 9, a slight modification of the method, previously used in Ref. 8 and 13, has also been applied in the present calculations.

Due to the boundary condition, eq. (3.9), it can be seen that the θ-momentum equation and the rate equation may be used in their exact forms. Hence, only two equations of the set, namely the conservation of mass and the r-momentum equation, are approximated by assuming a linear variation of certain integrands across the shock layer, thus permitting an integration of the equations in the direction of the radial coordinate, which in turn results in two ordinary differential equations with the tangential coordinate as independent variable. The integrands, for which a linear variation across the shock layer must be assumed, are

$$\rho u \qquad \rho uv, \text{ and } (p + \rho u^2) \tag{3.22}$$

Applying the above described linearization to the continuity and the r-momentum equation, and making use of the fact that the body contour is a streamline (eq. (3.9)), the complete set of governing equations for the flow past a circular cylinder can now be written as follows:

Continuity:

$$\rho_b \frac{du_b}{d\theta} + u_b \frac{d\rho_b}{d\theta} + \rho_s \frac{du_s}{d\theta} + u_s \frac{d\rho_s}{d\theta} =$$

$$= \frac{1+\epsilon}{\epsilon} \left[(\rho_b u_b - \rho_s u_s) \cot(\sigma + \theta) - 2\rho_s \bar{v}_s \right] \tag{3.23}$$

θ-momentum:

$$\rho_b u_b \frac{du_b}{d\theta} + \frac{dp_b}{d\theta} = 0 \tag{3.24}$$

r-momentum:

$$\frac{d}{d\theta}(\rho_s u_s v_s) = \frac{2+\epsilon}{\epsilon}(p_b - p_s) + \rho_b u_b^2 + \rho_s u_s^2$$

$$- \frac{1+\epsilon}{\epsilon} \left[\rho_s u_s v_s \cot(\sigma + \theta) + 2\rho_s v_s^2 \right] \tag{3.25}$$

Rate:

$$u_b \frac{d\alpha_b}{d\theta} = F_b r_b \tag{3.26}$$

Energy:

$$\frac{u_b^2}{2} + h_b = h_t = \frac{u_1^2}{2} + h_1 = \text{const.} \tag{3.27}$$

State:

$$p_b = \rho_b R Z_b T_b \tag{3.28}$$

In the above equations, use has already been made of eq. (3.21), in order to eliminate the derivative of Δ. Eq. (3.21) through (3.28) constitute a system of seven equations for the seven unknowns, which are u_b, ρ_b, p_b, T_b, α_b, $\epsilon = \Delta/r_b$, and σ. For the actual numerical integration, it is convenient to eliminate the derivatives of u_b and p_b. This reduces the system to the set of the following four differential equations:

Conservation of mass:

$$(u_b^2 - RZ_bT_b)\frac{d\rho_b}{d\theta} - \rho_b RZ_b \frac{dT_b}{d\theta} - \rho_b RbT_b \frac{d\alpha_b}{d\theta} + u_b \frac{d}{d\theta}(\rho_s u_s) =$$

$$= \frac{(1+\epsilon)u_b}{\epsilon}\left[(\rho_b u_b - \rho_s u_s)\cot(\sigma+\theta) - 2\rho_s v_s\right] \qquad (3.29)$$

θ-momentum:

$$RZ_bT_b \frac{d\rho_b}{d\theta} + \rho_b\left[RZ_b - \left(\frac{\partial h_b}{\partial T_b}\right)_{\alpha_b}\right]\frac{dT_b}{d\theta} + \rho_b\left[RT_b b - \left(\frac{\partial h_b}{\partial \alpha_b}\right)_{T_b}\right]\frac{d\alpha_b}{d\theta} = 0 \qquad (3.30)$$

plus the r-momentum and the rate equation as given in eq. (3.25) and (3.26). Once ρ_b, T_b, α_b, and σ are determined from eq. (3.25), (3.26), (3.29), and (3.30), the energy equation and the equation of state are used to calculate u_b and p_b, respectively.

3.4 Stagnation Streamline Conditions

Before the numerical integration of the system of equations for the flow around the circular cylinder can be started, the stagnation point parameters, serving as initial values, must be determined. For this purpose, the governing equations are specialized for the stagnation streamline, where $\theta = 0$ and $u_b = u_s = 0$. From eq. (3.5) through (3.8), one obtains, respectively,

Continuity:

$$\frac{d}{dr}(\rho v r) + \rho\left(\frac{\partial u}{\partial \theta}\right)_{\theta=0} = 0 \qquad (3.31)$$

θ-momentum:

$$\frac{dp}{d\theta} = 0 \qquad (3.32)$$

r-momentum:

$$r \frac{d}{dr} (p + \rho v^2) + \rho v \left[v + \left(\frac{\partial u}{\partial \theta} \right)_{\theta=0} \right] = 0 \tag{3.33}$$

Rate:

$$v \frac{d\alpha}{dr} - F = 0 \tag{3.34}$$

Energy:

$$\frac{v^2}{2} + h = h_t = \text{const.} \tag{3.35}$$

Together with the equation of state, eq. (3.31) and eq. (3.33) through (3.35) constitute a system of five equations for the five unknowns (p, ρ, T, α, and v) along the stagnation streamline. After some algebra, and after eliminating the derivatives of v and p, the following set of first order ordinary differential equations is obtained:

$$\frac{d\alpha}{dr} = \frac{F}{v} \tag{3.36}$$

$$\frac{dT}{dr} = \frac{p\left[v + \left(\frac{\partial u}{\partial \theta} \right)_{\theta=0} \right] - r\rho F \left[RTb - \left(\frac{\partial h}{\partial \alpha} \right)_T (1 - p/\rho v^2) \right]}{r\rho v \left[RZ - \left(\frac{\partial h}{\partial T} \right)_\alpha (1 - p/\rho v^2) \right]} \tag{3.37}$$

$$\frac{d\rho}{dr} = \frac{\rho}{v^2} \left\{ \left(\frac{\partial h}{\partial \alpha} \right)_T \frac{F}{v} + \left(\frac{\partial h}{\partial T} \right)_\alpha \frac{dT}{dr} - \frac{v}{r} \left[v + \left(\frac{\partial u}{\partial \theta} \right)_{\theta=0} \right] \right\} \tag{3.38}$$

Once α, T, and ρ are determined from the above equations, u and p are obtained from the energy equation and from the equation of state, respectively.

Equations (3.36) through (3.38) still contain the unknown gradient of u in θ direction, which for fixed θ is a function of the radial coordinate r only. In order to determine this gradient, use is made of the linear approximation for ρu, which was previously needed in order to derive eq. (3.23). The first order polynomial

approximation for ρu is, in general,

$$\rho u = (\rho u)_b + [(\rho u)_s - (\rho u)_b] \frac{r - r_b}{\Delta} \tag{3.39}$$

Differentiating the above expression with respect to θ, and specializing the resulting equation for the stagnation streamline ($\theta = 0$, $u = u_b = u_s = 0$), one obtains

$$\rho \left(\frac{\partial u}{\partial \theta} \right)_{\theta=0} = \rho_b \left(1 - \frac{\eta - 1}{\epsilon_o}\right) \left(\frac{du_b}{d\theta} \right)_{\theta=0} + \rho_s \left(\frac{\eta - 1}{\epsilon_o} \right) \left(\frac{du_s}{d\theta} \right)_{\theta=0} \tag{3.40}$$

where $\eta = r/r_b$ is the nondimensionalized radial coordinate r, having the range $1 \leq \eta \leq 1 + \epsilon_o$. Eq. (3.40) contains three gradients which can be determined as follows:

Specializing the approximate continuity equation, eq. (3.23), for $\theta = 0$, one can solve for

$$\rho_b \left(\frac{du_b}{d\theta} \right)_{\theta=0} = - \frac{2 + \epsilon_o}{\epsilon_o} \rho_s v_s - \rho_s u_1 \left(\frac{\rho_1}{\rho_s} - 1 \right) \left(\frac{d\sigma}{d\theta} \right)_{\theta=0} \tag{3.41}$$

Differentiating eq. (3.17) with respect to θ, and then specializing for $\theta = 0$, one obtains

$$\left(\frac{du_s}{d\theta} \right)_{\theta=0} = u_1 \left(\frac{\rho_1}{\rho_s} - 1 \right) \left(\frac{d\sigma}{d\theta} \right)_{\theta=0} - v_s \tag{3.42}$$

Finally, solving the approximate r-momentum equation, eq. (3.25), for the gradient of σ, and then specializing the result for the stagnation streamline, one arrives at

$$\left(\frac{d\sigma}{d\theta} \right)_{\theta=0} = \frac{(2 + \epsilon_o)(p_b - p_s) - (2 + \epsilon_o)\rho_s v_s^2}{v_s u_1 \epsilon_o (\rho_1 - \rho_s)} \tag{3.43}$$

Substituting now the last three expressions into eq. (3.40), it can be shown that

$$\left(\frac{\partial u}{\partial \theta}\right)_{\theta=0} = \frac{2\rho_s v_s^2(1+\epsilon_o)(\eta-1) + (p_b - p_s)(2+\epsilon_o)[\epsilon_o - 2(\eta-1)]}{-\rho v_s \epsilon_o^2} \tag{3.44}$$

The above is seen to be a function of the radial coordinate η, the conditions behind the shock, the stagnation point pressure p_b, and the stagnation point shock detachment distance ϵ_o. Hence, the system (3.36) through (3.38), together with the energy equation, the equation of state, and eq. (3.44), can now be solved for an assumed stagnation point pressure, for which a first guess is obtained from a constant density calculation (Ref. 16). Also assuming a value for ϵ_o, the system is then integrated and iterated on p_b, until the assumed value of p_b agrees with the value resulting from the integration.

3.5 Numerical Techniques

For both the integration along the stagnation streamline and the integration along the body surface, a fixed step Runge-Kutta technique of fourth-order accuracy was used. A thousand steps were chosen for the stagnation streamline; for the integration around the body, the step size was fixed at 0.002 radians, corresponding to roughly 0.1 degrees. All calculations were performed on a UNIVAC 1107 high speed digital computer.

Having determined the stagnation point conditions as described in section 3.4, the integration around the body is started with an assumed

shock detachment distance ϵ_o. The equations for the body surface variables are strongly dependent on this value, and smooth transitions of all variables from the subsonic to the supersonic flow regime are only obtained for a correctly chosen ϵ_o. Depending on the case, between ten and fifteen iterations were needed to determine ϵ_o to four significant figures. Near the point where the surface velocity reaches the local speed of sound, the equations have a singularity; and the behavior of the solution becomes badly nonlinear. For the case of frozen and equilibrium flow, the singularity occurs at the sonic point; however, this is not true for non-equilibrium flow (Ref. 8). Previous investigators (Ref. 3, 8, 10) have reported that the singularity is of the saddle-point type. In the present formulation of the problem, this was not apparent; and more research in this direction seems to be necessary.

Once a smooth distribution of all variables in the entire subsonic region was obtained, all dependent variables were extrapolated into the supersonic region by using a second order polynomial curve fit. The integration was then resumed and could, in most cases, be carried out up to the shoulder of the body, in some cases even farther.

DISCUSSION OF RESULTS

4.1 Stagnation Streamline

Numerical results have been obtained for a number of cases, only a few of which can be discussed here. For chemical non-equilibrium flow, the degree of dissociation and the temperature are particularly interesting parameters. Fig. 2 and 3 show the distribution of α and T, respectively, along the stagnation streamline behind the bow shock for a flight speed of 4300 m/sec at an altitude of 30 km. It can be seen that, depending on the size of the body, quite different regimes of non-equilibrium flow are encountered. For relatively large bodies, the local chemical relaxation time is short compared to a characteristic flow time which causes the flow to reach the state of thermodynamic equilibrium close behind the shock. On the other hand, for very small bodies, the relaxation time becomes large if compared to a characteristic flow time. In this case, the flow remains essentially frozen and equilibrates only near the stagnation point, where the velocity approaches zero and the relaxation time is again small compared to the local residence time of a flow particle. It was found that, under all circumstances, the flow always reaches thermodynamic equilibrium at the stagnation point.

In both figures the present results from the integral method are compared with data calculated by Conti (Ref. 17), who used an inverse method and also different reaction rate constants. The air model was the same as ours.

4.2 Flow Around Circular Cylinder

It is already well known from perfect gas calculations that with increasing free stream Mach numbers the bow shock moves closer to the body. It is seen from Fig. 4 and 5 that in chemical non-equilibrium flow this trend is retained. Both figures also indicate clearly that dissociation of the free stream, keeping all other free stream parameters unchanged, causes the bow shock to move away from the body. One reason for this effect is that, for a dissociated free stream, the density behind the shock is lower than for corresponding conditions without free stream dissociation (Ref. 15). The effect is seen to increase with decreasing free stream Mach number. Fig. 4 also shows that the shock shape deviates considerably from a concentric circle, even where the velocity in the shock layer is still subsonic.

From Fig. 5 it is observed that the present calculations yield a stagnation shock detachment distance which is much smaller, even for an undissociated free stream, than the values obtained from perfect gas calculations (Ref. 3, 6). Responsible for this effect is our assumption of vibrational equilibrium throughout the flow field. It is shown that, for a free stream Mach number of $M_1 = 3$, where the bow shock does not yet cause appreciable molecular vibration in the shock layer, the present calculation predicts a value which is very close to the known perfect gas result. Again, it is gratifying to see that for the high Mach number range ($M_1 = 14.2$) our results agree closely with those of Conti (Ref. 17), which were obtained by an entirely different approach.

The velocity distribution along the surface of the cylinder, as evident from Fig. 6, is almost linear up to the sonic point. A distinct effect of free stream dissociation can be seen.

The degree of oxygen dissociation along the non-catalytic body surface is presented in Fig. 7. Especially for the high Mach number cases, it is seen that the recombination process dominates in the subsonic regime as the flow expands around the body. The degree of dissociation decreases slowly until, in the supersonic regime, the local residence time of a particle becomes so small compared to the relaxation time that the flow freezes. With lower free stream Mach numbers, this effect becomes less pronounced until, for the lowest case shown, no change in composition at all is observed. For a better understanding, however, the non-equilibrium results should be compared to those for equilibrium flow and frozen flow, which are not available at the present time.

Finally, Fig. 8 and 9 show the temperature and the pressure distribution along the surface of the cylinder for selected free stream Mach numbers with and without dissociation of the free stream. As expected, free stream dissociation has a strong effect on the temperature but practically no effect on the pressure. Therefore, pressure distributions are presented only for zero free stream dissociation.

4.3 Concluding Remarks

Hypersonic non-equilibrium flow of air past a circular cylinder was investigated,using Dorodnitsyn's method of integral relations.Air was represented by a simplified model consisting of a three component reacting gas.

Results were presented for a wide range of free stream Mach numbers. The investigation included an analysis of the flow along the stagnation streamline.It was shown in particular that the size of the body has a decisive influence on the distribution of temperature and degree of dissociation along the stagnation streamline.

The solution for the flow along the surface of the circular cylinder was extended far into the supersonic regime up to the shoulder of the body.It was found that dissociation of the free stream , as it may occur either in the atmosphere at high altitudes, or in the nozzle of heated flow facilities, has a strong effect on the shock detachment distance , as well as on the distribution of velocity, dissociation, density , and temperature along the body surface. The body surface pressure was shown to be in close agreement with the Modified Newtonian Theory , and hardly influenced at all by free stream dissociation.

ACKNOWLEDGEMENT

The authors wish to express their sincere appreciation to Mr. Robert A. McGraw and to Mr. Otis Vaughn for programming this problem.

REFERENCES

1. Hall, J. G., Eschenroeder, A. G., and Marrone, P. V., "Inviscid Hypersonic Airflows With Coupled Nonequilibrium Processes," Cornell Aeronautical Laboratory, Rep. No. AF-1413-A-2, 1962.

2. Dorodnitsyn, A. A., "A Contribution to the Solution of Mixed Problems of Transonic Aerodynamics," Advances in Aeronautical Sciences, Vol. 2, Pergamon Press, New York, 1959, pp. 832-844.

3. Belotserkovskii, O. M., "Flow Past a Circular Cylinder With a Detached Shock Wave," Doklady Akad. Nauk SSSR 113, No. 3, 1957. Also AVCO RAD-9-TM-59-66, 1959.

4. Holt, M., "Calculation of Pressure Distribution on Hypersonic Bodies by Belotserkovskii's Method," AVCO RAD-2-TM-58-45, 1958.

5. Traugott, S. C., "An Approximate Solution of the Supersonic Blunt Body Problem for Prescribed Arbitrary Axisymmetric Shapes," Martin Company, Res. Rep. No. 13, 1958.

6. Archer, R. D., "Inviscid Supersonic Flow Around an Elliptic Nose," Ph.D. Thesis, University of Minnesota, November 1963.

7. Yalamanchili, J., Hermann, R., "Non-Equilibrium Hypersonic Flow of Air in Hypersonic Nozzles and Around Blunt Bodies," University of Alabama Research Institute, Res. Rep. No. 3, May 1963.

8. Shih, W. C. L., Baron, J. R., Krupp, R. S., and Towle, W. J., "Nonequilibrium Blunt Body Flow Using the Method of Integral Relations," Massachusetts Institute of Technology, Aerophysics Lab., Tech. Rep. 66. Also DDC AD No. 415 934, May 1963.

9. Hermann, R., Yalamanchili, J., "Hypersonic Flow With Non-Equilibrium Dissociation Around Blunt Bodies in Flow Facilities and in Free Flight," WGLR Yearbook, 1963.

10. Belotserkovskii, O. M., Golomazov, M. M., Shulishnina, N. D., "Calculation of Flow of Dissociated Air in Equilibrium Around Blunt Bodies With Detached Shock Wave," JCMMP, Vol. 4, No. 2, March-April 1964, pp. 306-316.

11. Hermann, R., "Hypersonic Flow Problems During Re-Entry Into the Atmosphere," WGLR Yearbook, 1961.

12. Hermann, R., Thompson, K. O., and Yalamanchili, J., "An Analytical Study of the Effects of Dissociation of High Temperature Air at Hypersonic Velocities Around Blunt Bodies and Study of Design Requirements of Arc Heated Hypersonic Wind Tunnels," University of Minnesota, Rosemount Aeronautical Lab., Res. Rep. No. 185, 1962.

13. Thoenes, J., "Inviscid High Temperature Hypersonic Flow of Air Past Pointed Bodies of Revolution," University of Alabama Research Institute, Res. Rep. No. 25, 1965.

14. Wray, K. L., "Chemical Kinetics of High Temperature Air," in "Hypersonic Flow Research," Progress in Astronautics and Rocketry, Vol. 7, Academic Press, 1962.

15. Yalamanchili, J., Thoenes, J., "Normal and Oblique Shock Wave Parameters for Various Dissociated Upstream Conditions in Air With Frozen Composition Across the Shock," University of Alabama Research Institute, Res. Rep. No. 4, 1964.

16. Truitt, W. T., "Hypersonic Aerodynamics," The Ronald Press Company, New York, 1959.

17. Conti, R. J., "Stagnation Equilibrium Layer in Nonequilibrium Blunt-Body Flows," AIAA Journal, Vol. 2, November 1964, pp. 2044-2046.

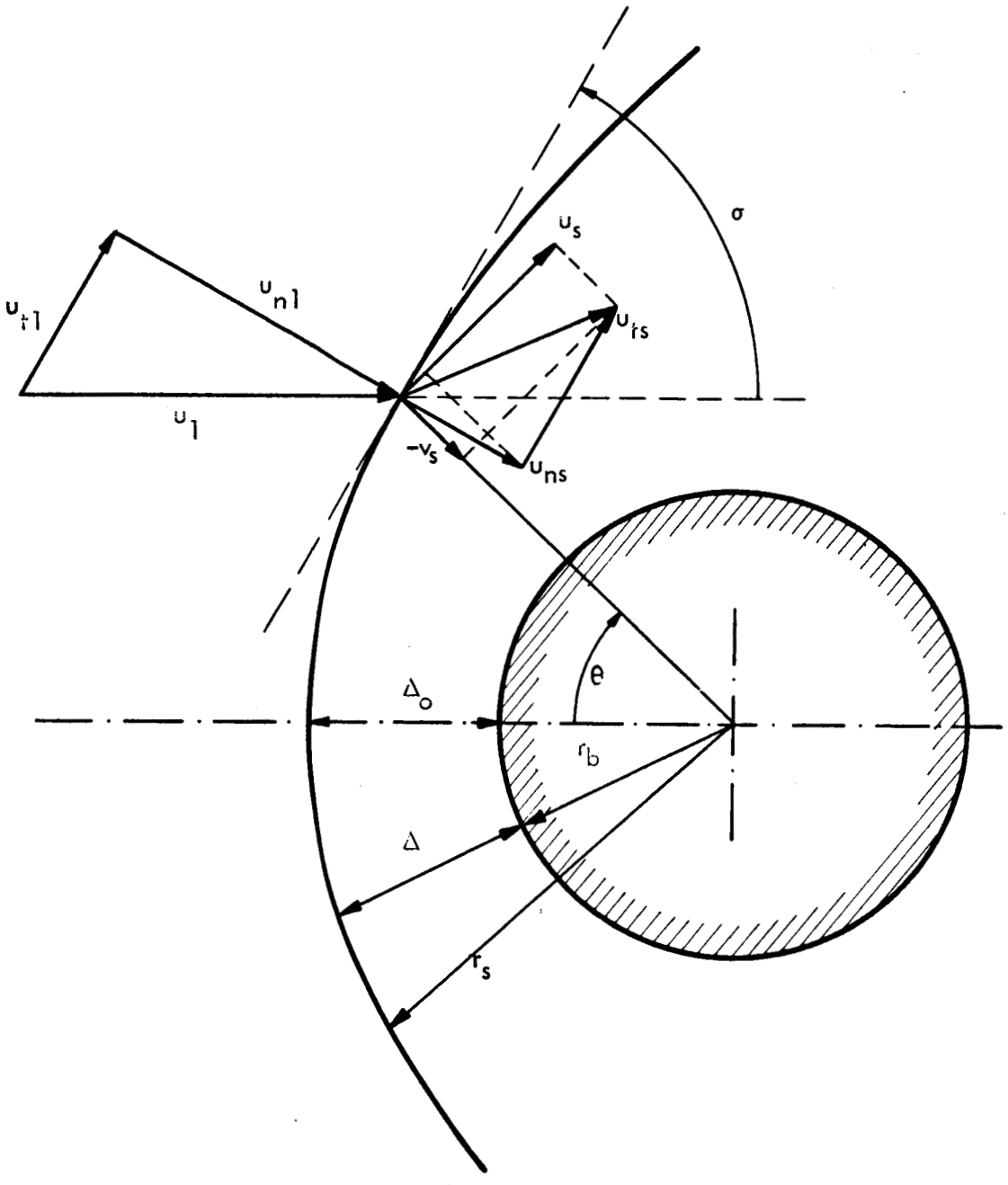

FIG. 1 COORDINATE SYSTEM AND SHOCK WAVE GEOMETRY ON CIRCULAR CYLINDER

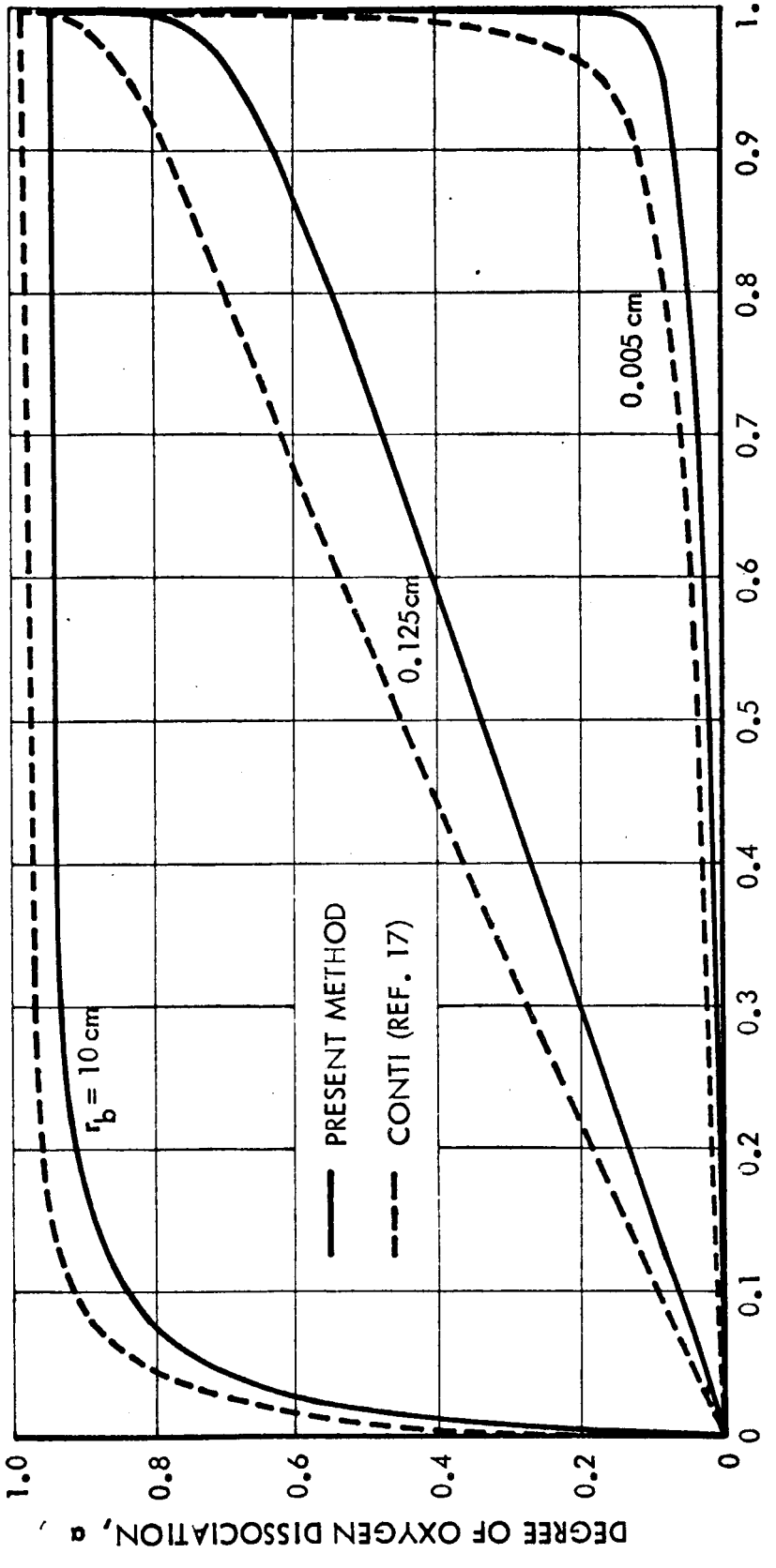

FIG 2 DEGREE OF OXYGEN DISSOCIATION ALONG STAGNATION STREAMLINE FOR VARIOUS BODY RADII (Flight Speed 4300 m/sec, Altitude 30 km)

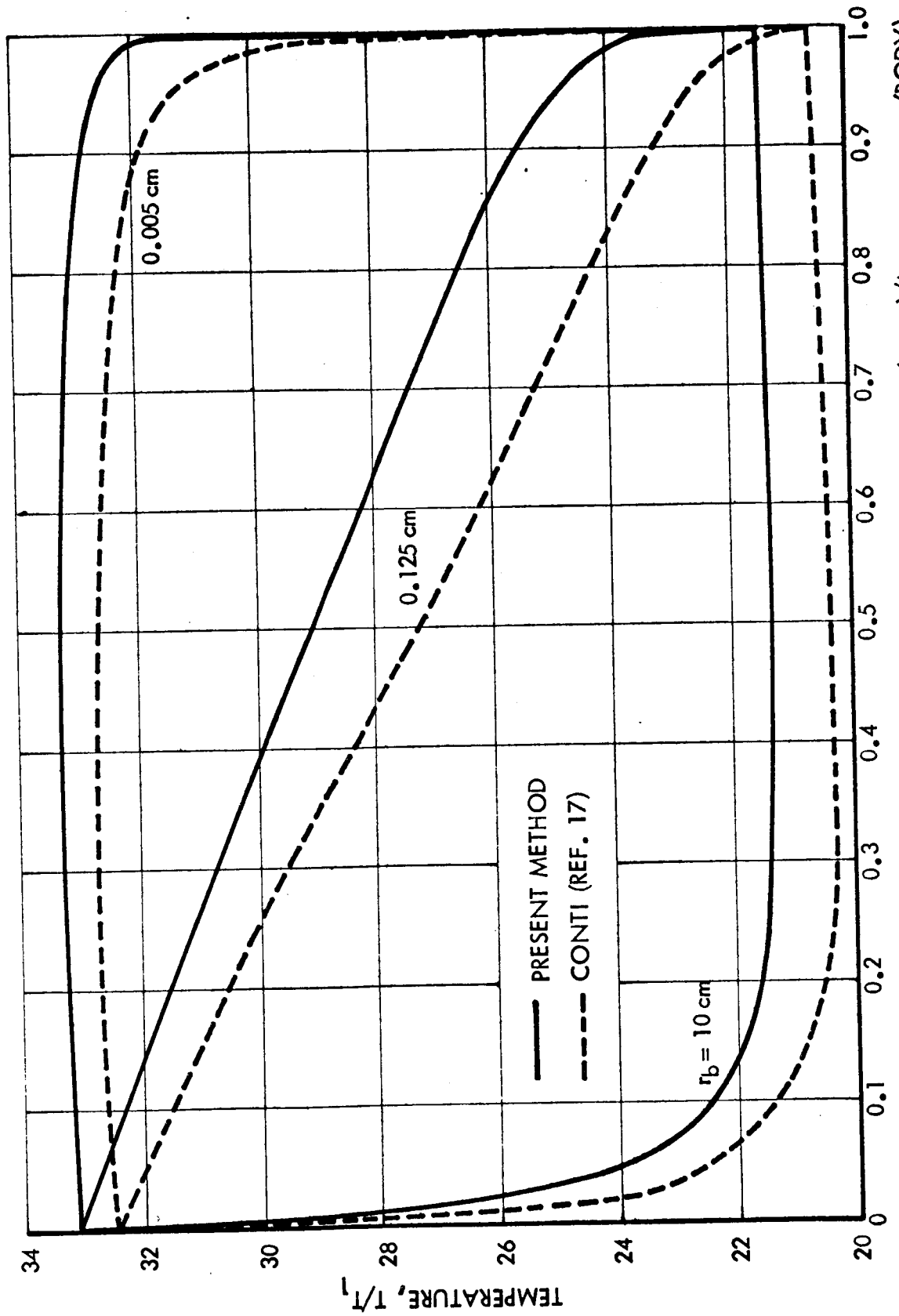

FIG. 3 TEMPERATURE ALONG STAGNATION STREAMLINE FOR VARIOUS BODY RADII (Flight Speed 4300 m/sec, Altitude 30 km)

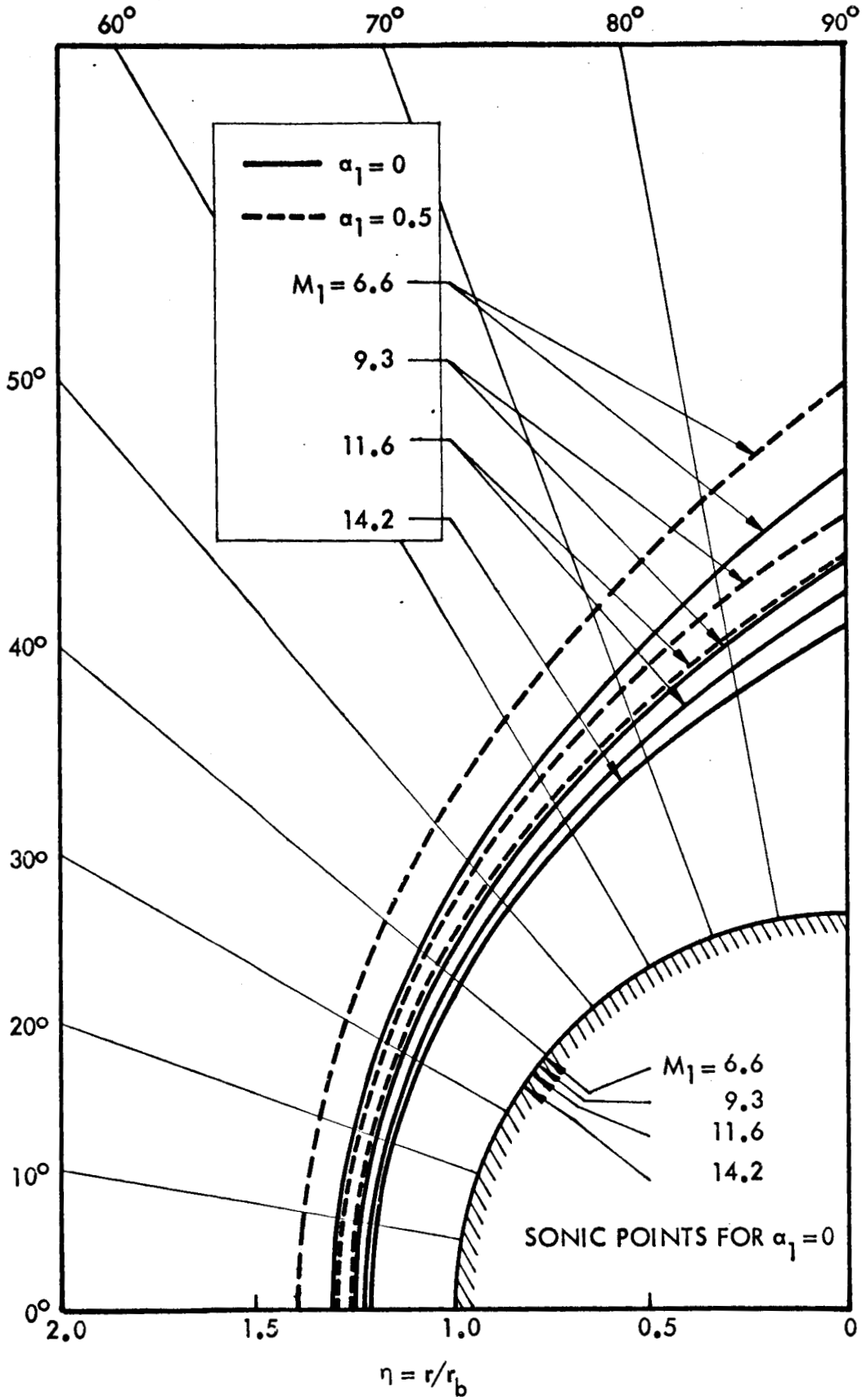

FIG. 4 CALCULATED SHOCK SHAPES FOR CIRCULAR CYLINDER (r_b = 10 cm, Altitude 30 km)

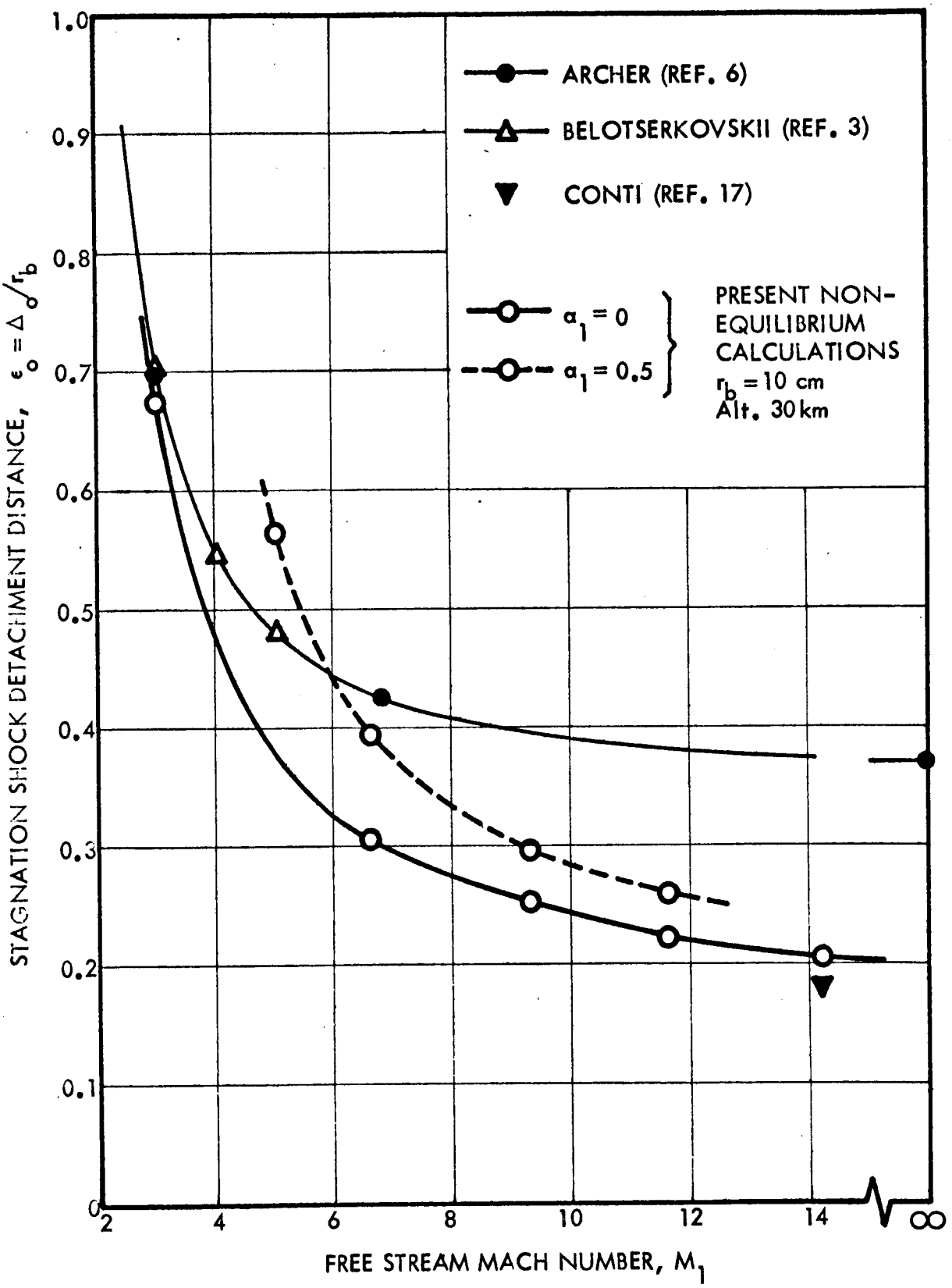

FIG. 5 STAGNATION SHOCK DETACHMENT DISTANCE ON CIRCULAR CYLINDER

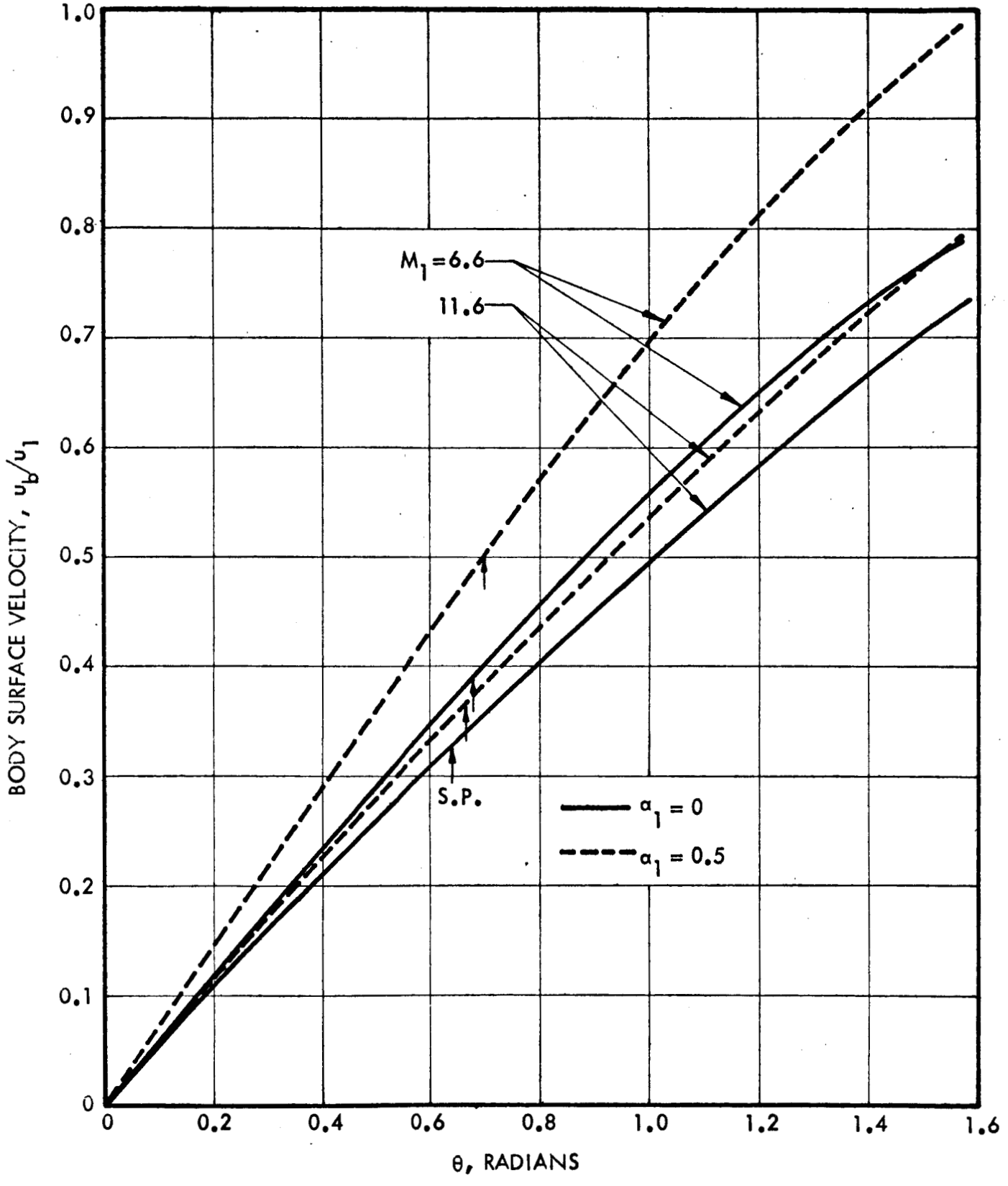

FIG. 6 VELOCITY DISTRIBUTION ALONG BODY SURFACE (r_b = 10 cm, Altitude 30 km)

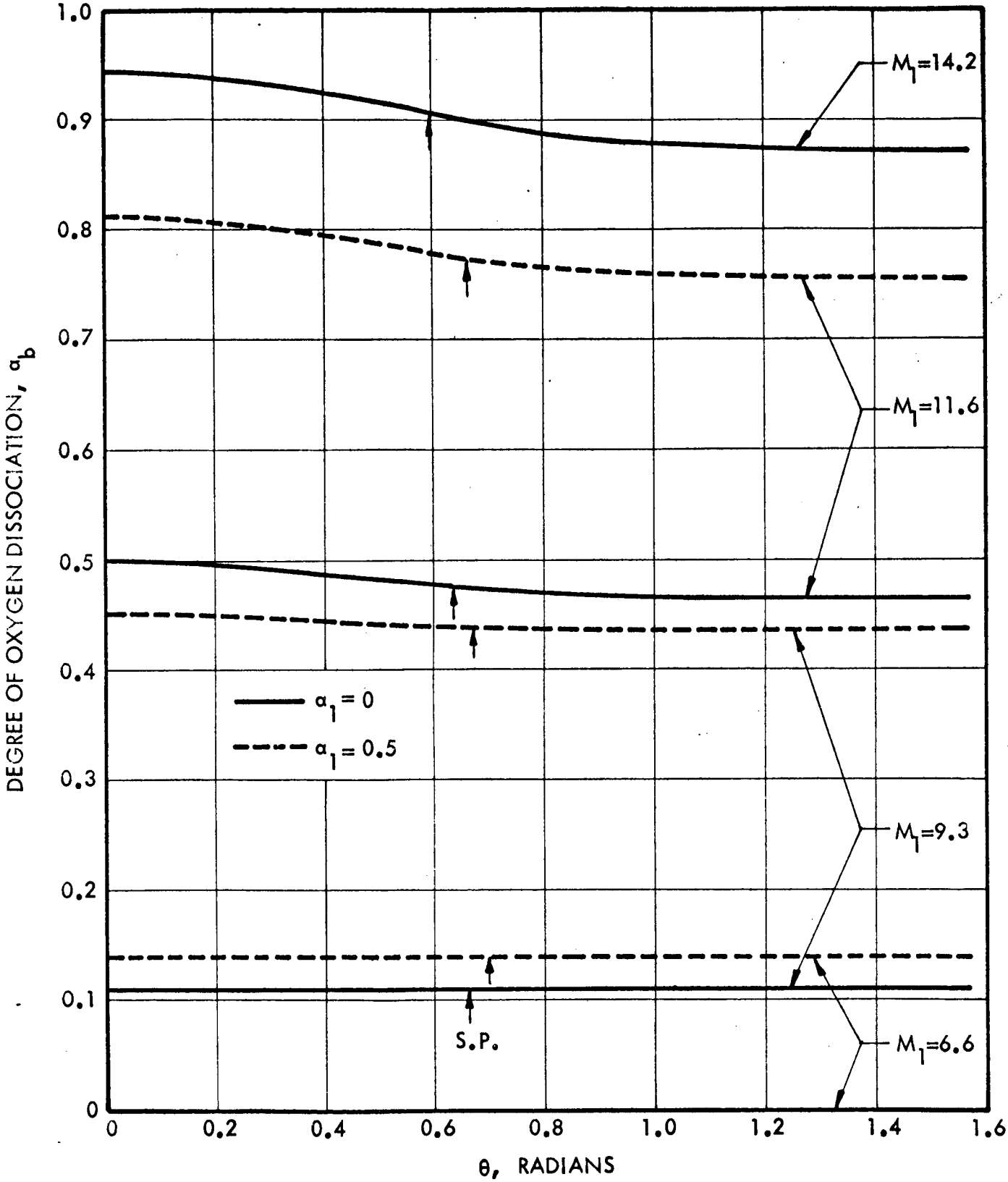

FIG. 7 DEGREE OF OXYGEN DISSOCIATION ALONG BODY SURFACE
(r_b = 10 cm, Altitude 30 km)

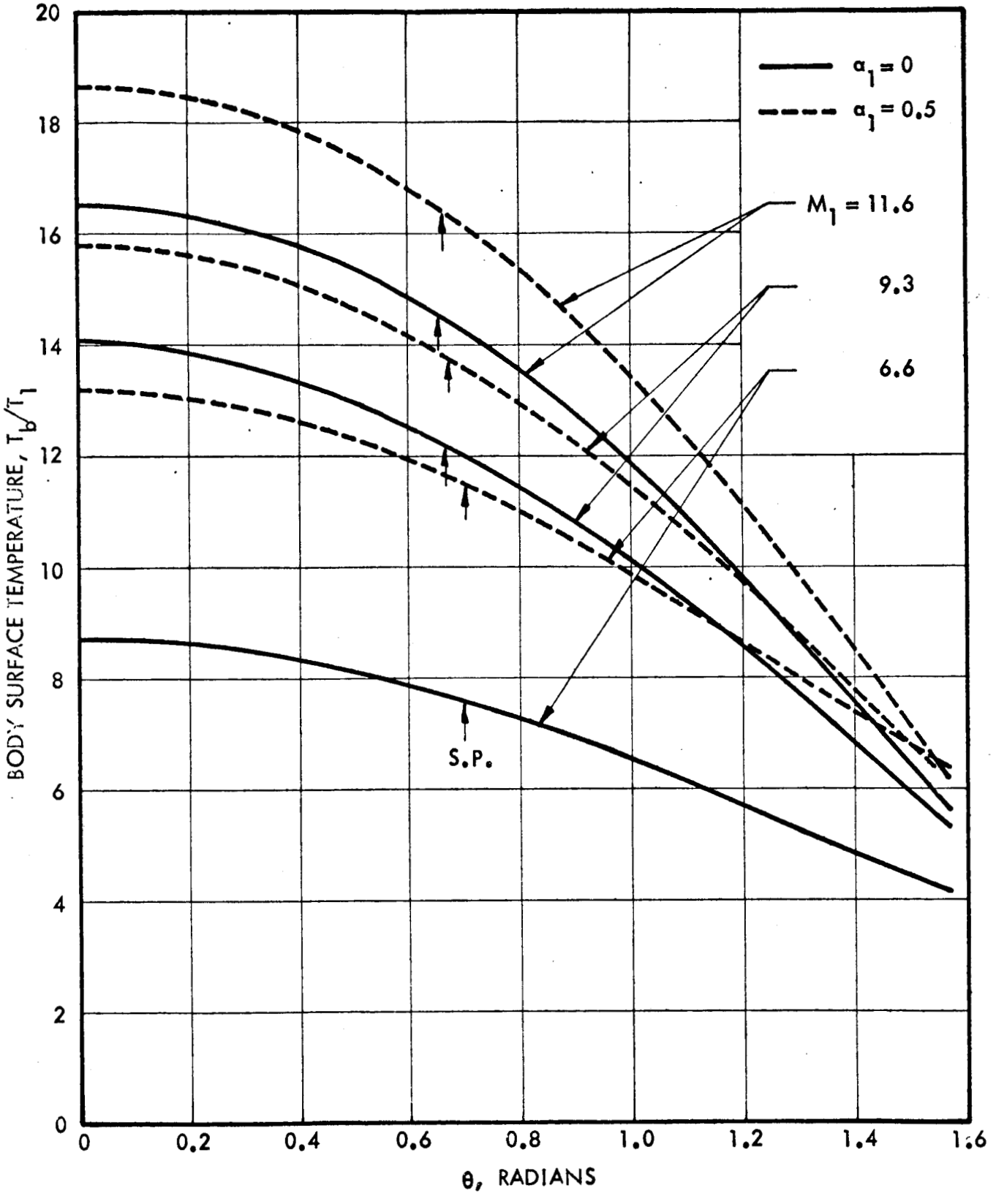

FIG. 8 TEMPERATURE DISTRIBUTION ALONG BODY SURFACE (r_b = 10 cm, Altitude 30 km)

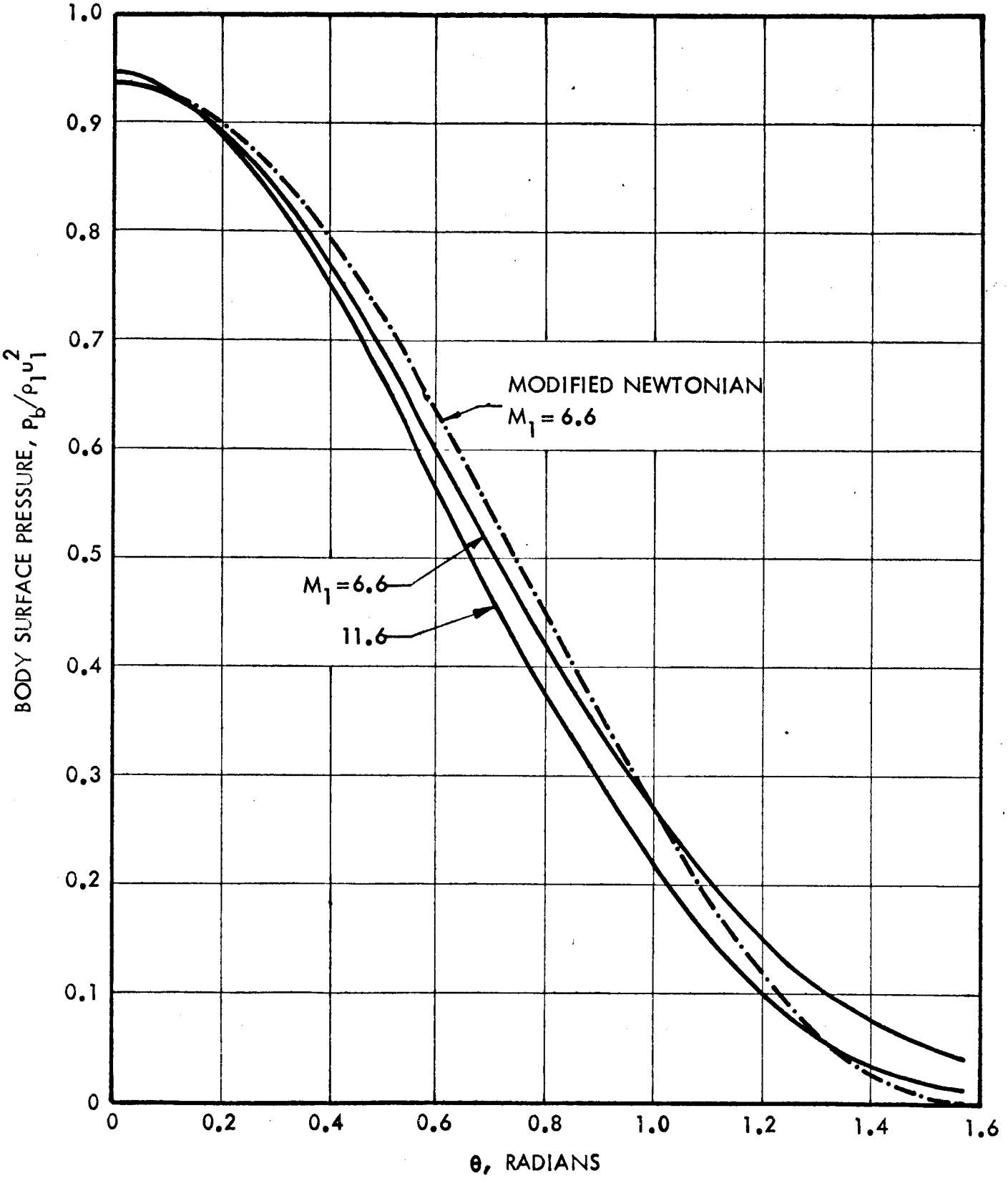

FIG. 9 PRESSURE DISTRIBUTION ALONG BODY SURFACE (r_b = 10 cm, Altitude 30 km)